Journal of *Marine Science and Engineering*

MDPI

Article

Experimental and Numerical Investigation of the Added Resistance in Regular Head Waves for the DTC Hull

Ana-Maria Chirosca [1], Antonio Medina [2], Florin Pacuraru [3,*], Simone Saettone [2], Liliana Rusu [1] and Sandita Pacuraru [3]

[1] Department of Mechanical Engineering, Faculty of Engineering, "Dunarea de Jos" University of Galati, 47 Domneasca Street, 800008 Galati, Romania; ana.chirosca@ugal.ro (A.-M.C.)
[2] CEHINAV, DACSON, ETSIN, Universidad Politécnica de Madrid (UPM), 28040 Madrid, Spain
[3] Department of Naval Architecture, Faculty of Naval Architecture, "Dunarea de Jos" University of Galati, Domneasca Street 111, 800201 Galati, Romania
* Correspondence: florin.pacuraru@ugal.ro

Abstract: Reducing the added resistance in waves has become a crucial aspect of today's ship design. The added resistance in waves is traditionally considered proportional to the square of wave height. However, this assumption is believed to be only partly valid, and further investigations are required. In the present study, experimental tests and numerical simulations were carried out to determine the added resistance in regular head waves of the DTC hull (the scale factor is 135). The numerical analysis was performed with SHIPFLOW 7.01, and the experimental campaign was carried out in the ETSIN-UPM towing tank. The investigation revealed that the added resistance in waves was not proportional to the square of the wave height, and a better correlation was obtained by changing the power of the wave weight to 1.75. Furthermore, an unexpected double resonance phenomenon on the added resistance was found at a Froude number of 0.13. The study also revealed an acceptable agreement between the numerical simulations and the experiments, except for the double resonance phenomenon.

Keywords: DTC; numerical; experimental; added resistance in waves; regular waves; head waves; validation

Citation: Chirosca, A.-M.; Medina, A.; Pacuraru, F.; Saettone, S.; Rusu, L.; Pacuraru, S. Experimental and Numerical Investigation of the Added Resistance in Regular Head Waves for the DTC Hull. *J. Mar. Sci. Eng.* **2023**, *11*, 852. https://doi.org/10.3390/jmse11040852

Academic Editors: Simone Mancini and Momchil Terziev

Received: 16 March 2023
Revised: 14 April 2023
Accepted: 16 April 2023
Published: 18 April 2023

1. Introduction

The shipping industry is vital for the global economy, since approximately 80% of the international merchandise trade volume is carried by sea. On the other hand, the maritime sector is responsible for around 2.5% of the world's total CO_2 emissions. As a response, the International Maritime Organization has set a target to cut these emissions by 50% by 2050 compared to 2008 levels. The International Maritime Organization enforced three energy efficiency indexes to meet its emission reduction goal: the Energy Efficiency Design Index (EEDI), the Carbon Intensity Indicator (CII), and the Energy Efficiency Existing Ship Index (EEXI). The requirements imposed by these indexes can be met by improving the ship's hydrodynamic performance. As a result, reducing the added resistance in waves has become a critical aspect of increasing the ship's energy efficiency. Furthermore, the precise estimate of the added resistance in waves is crucial to optimize the ship's route.

A prediction of the added resistance in waves can be made through several techniques, such as numerical simulations and experimental testing [1]. Perhaps the earliest attempt at the numerical estimation of the added resistance in waves was made by Havelock [2]. Further studies have been reported by Maruo [3–5], who introduced the first far-field approach based on the momentum conservation theory to estimate the added resistance in waves by the wave energy and momentum fluxes around the hull. This method was further developed by Joonsen [6] and later by Gerritsma and Beukelman [7], who elaborated on the radiated energy approach, where the drift force is proportional to the amplitude of the radiated wave in the far field. Later, Salvesen [8] combined this method with the strip

theory [9], which led to better results in terms of motions and added resistance in waves. On the other hand, Boese [10] and Faltinsen [11] elaborated the near-field approaches based on hull pressure integration. Since then, more strip theory variations have been developed [12–17]. Despite theoretical shortcomings, strip theory has the advantage of being fast, inexpensive, and sufficiently accurate for several practical applications.

Efforts to model more complex phenomena (e.g., nonlinear applications) led to the development of other potential flow alternatives based on 3D numerical methods. Essentially, two methods were developed based on the type of singularities used in the integral equations. One approach is usually based on the frequency domain and uses Green's function, which automatically satisfies the radiation and linearized free surface conditions [18–20]. The second approach relies on distributing the Rankine sources on the hull and free surfaces [21–26]. Furthermore, hybrid singularity distributions of Rankine sources in the inner domain and transient Green's function in the outer domain have also been applied [27–29].

The development of computational resources has facilitated the use of computational fluid dynamics (CFD) techniques for predicting the added resistance in waves. Compared to potential flow methods, CFD methods can deal with problems in steep waves and flow details [30,31]. The treatment of the free surface in a RANS (Reynolds-averaged Navier–Stokes equation) computation of an advancing ship in waves is crucial. The interface capturing approach, such as volume of fluid (VOF) [32] or the level-set method [33], enables the computing of the free surface elevation by solving transport equations for a distance function or the fraction of a control volume. This approach opened the door to simulating ship motions in waves numerically. Several studies on validating the added resistance in waves based on RANS include the works of [34–38]. Liu et al. [29] compare the DTC ship seakeeping numerical results obtained using a 3D panel method NEWDRIFT+ of NTUA-SDL with corresponding experimental data generated within the SHOPERA project (2013–2016) at MARINTEK for various wave headings at low-to-moderate speeds. Kobayashi et al. [39] recently conducted comprehensive parametric studies concerning the added resistance in head waves using an overset approach based on a structured grid for the DTC (Duisburg Test Case) and JBC (Japan Bulk Carrier) hulls. The research also recommended configurations for domain size, grid resolution, and computational conditions. Although RANS methods are still too computationally expensive to account for larger parameter variations, potential flow methods are still widely used to predict the additional wave resistance in the early design phase [18].

Experimental investigations of the added resistance in waves have been conducted for decades. One of the first and most significant experimental campaigns is the systematic work on 16 different Series 60 hull forms by Vossers et al. [40,41]. Other relevant experimental studies were conducted by Sibul [42,43], Longo and Stern [44], Irvine et al. [45], Park et al. [46], Sogihara et al. [47], and Saettone [48]. Moreover, a few recent studies focused on reducing added resistance by examining the effects of bow shape on added resistance and motion responses [49–54].

In terms of comparative studies, various added resistance estimation approaches have been analyzed in order to determine reliability of each method. For example, the study of Shigunov et al. [55] provides a comprehensive summary of the results from an international benchmark study on numerical methods for predicting time-average wave-induced forces and insight into accuracy and reliability across various test cases. The strip, Rankine panel, and Cartesian-grid methods were compared in terms of accuracy and computational efficiency by Seo et al. [56,57]. Most recently Jae-Hoon et al. [58] compared several numerical computation methods, such as Asymptotic Formula, 2D Strip Theory, 3D Panel Method, and CFD, to investigate the accuracy and reliability among different analysis techniques with respect to physical aspects causing additional resistance due to a wave's impact on the ship's movement.

The quadratic trend of the added resistance with wave amplitude is a traditional assumption, meaning that the added resistance increases proportionally with the square of

the wave amplitude. However, the work of Yasukawa et al. [59] on three ship hulls with different block coefficients (0.81 to 0.87) showed that added resistance coefficient tends to be larger at lowest wave heights. This result indicated that, for the case of studies, the added resistance was not proportional to the wave height square. This phenomenon was believed to be caused by the loss of wave energy due to the breaking of the incident waves at the bow. The CFD and experimental analysis of Crepier et al. [27] for two hull forms sailing in head waves also suggested that the quadratic relationship between the wave amplitude and added resistance is only partly valid. The work of Dallinga [60] revealed that the peak value of the quadratic transfer function (QTF) of the added resistance of ships with a large flare decreased with the wave height. Martic et al. [61] numerically determined that the added resistance in waves of the DTC container ship in finite water was not proportional to the square of the wave amplitude. In addition, artificial intelligence is being applied for the evaluation of added resistance of container ships in head waves [62,63]. All the previous works indicate that the added resistance of the ship might not be proportional to the wave height square but increases at a slower rate. However, the phenomenon is not clearly understood yet, and further investigations are required. Specifically, additional experimental studies are necessary to understand the causes behind the non-quadratic behaviour. Furthermore, it is also necessary to understand if the potential flow theory is sufficiently accurate to reproduce the phenomenon adequately.

In the present study, towing-tank experiments and numerical simulations were carried out to investigate the quadratic behaviour of the added resistance coefficient and wave amplitude. The DTC hull was selected as the test case. A combination of seven wavelengths, three wave heights, and three Froude numbers was chosen. The experimental campaign was performed at the ETSIN-UPM (Escuela Técnica Superior de Ingeniería de Montes, Universidad Politécnica de Madrid) towing tank. Repeated tests were performed to determine the repeatability uncertainty. A 3D fully non-linear time-domain-based Rankine panel method was applied for the numerical analysis. The commercial SHIPFLOW package version 7.01 was used as the numerical tool. The results were then used for validation to gain an insight into the computation capability of the potential-based numerical model employed.

2. Geometry and Conditions

The Duisburg Test Case Hull, a Post-Panamax container ship [64], was selected as the case study. Based on the publicly available IGES (Initial Graphics Exchange Specification) geometry, a 1:135 scale model was constructed at "Dunarea de Jos" University and used for the experimental campaign. The model was made from PLA (Polylactic Acid) filament and 3D printed in several small sections (Figure 1) that were combined to create the final hull.

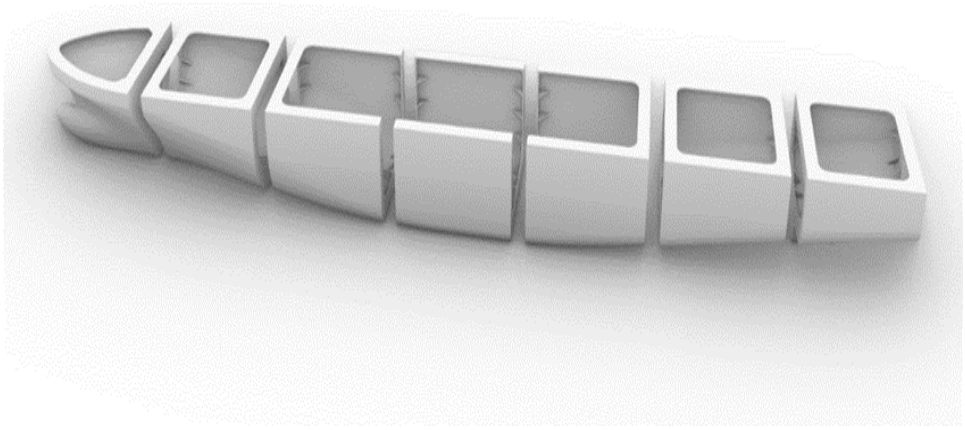

Figure 1. DTC Hull.

The experimental model consisted of seven blocks that were fastened together using M5x16 bolts and M5 nuts. To ensure a secure connection between the blocks, washers were used to increase the contact area of the nuts and bolts on the plastic flange. The blocks were impermeable after being 3D printed, apart from the connection point where water could potentially enter the hull. To prevent water leakage, a silicone sealant was applied during the assembly of the entire hull.

As can be seen in Figure 1, the vessel under study is a bare hull vessel with a bulbous bow, a large stern overhang, and a transom. The main features, both for the full scale and for the 1:135 model, are shown in Table 1.

Table 1. Main hull characteristics.

Main Dimensions			Full-Scale	Model-Scale
Scale	λ	-	-	135
Length between perpendiculars	L_{PP}	m	355	2.630
Waterline breadth	B_{WL}	m	51	0.378
Draught midship	T	m	14.5	0.107
Volume displacement	∇	m^3	173,467	0.071
Block coefficient	c_B	-	0.661	0.661
Wetted surface	S_w	m^2	22,032	1.209
Design speed	V	m/s	12.86	1.107
Longitudinal centre of buoyancy measured from the transom	X_{CB}	m	-	1.339
Longitudinal centre of buoyancy—from aft perpendicular	X_{CB}	m	-	1.289
Vertical centre of buoyancy—from baseline	Z_{CB}	m	-	0.059
Longitudinal centre of flotation—measured the from transom	X_{CF}	m	-	1.242
Longitudinal centre of gravity—from aft perpendicular	X_{CG}	m	174.059	1.289
Vertical centre of gravity—from aft perpendicular	Z_{CG}	m	19.851	0.147
Radius of gyration	ryy	m	87.4	0.647

The DTC model was tested in calm water conditions and in regular head waves for three ship speeds. A combination of seven wavelengths and three wave heights was selected for the test cases in waves. Table 2 shows the complete test matrix implemented in the current experimental campaign.

Table 2. Test case overview in model-scale.

Type	Speed	Dimensionless Wave Length	Wave Height	Wave Period
	v [m/s]	λ_w/L_{PP} [-]	H_w [m]	T_w [s]
Calm water	0.664, 0.885, 1.107	—	—	—
Regular head waves	0.664, 0.885, 1.107	0.500	0.030, 0.044, 0.057	0.918
	0.664, 0.885, 1.107	0.750	0.030, 0.044, 0.057	1.124
	0.664, 0.885, 1.107	0.875	0.030, 0.044, 0.057	1.214
	0.664, 0.885, 1.107	1.000	0.030, 0.044, 0.057	1.298
	0.664, 0.885, 1.107	1.125	0.030, 0.044, 0.057	1.377
	0.664, 0.885, 1.107	1.250	0.030, 0.044, 0.057	1.451
	0.664, 0.885, 1.107	1.500	0.030, 0.044, 0.057	1.590

3. Experimental Setup

3.1. Towing Tank

The experimental campaign was conducted in the ETSIN-UPM towing tank, whose dimensions are:

- Length: 100 m;
- Width: 3.8 m;
- Depth in the current experiments: 2.2 m.

The towing tank includes a running carriage with a maximum speed of 4 m/s. Regular and irregular waves can be generated by an elevated hinged single-flap wavemaker placed at one end of the tank. At the opposite end is a passive wave absorption.

3.2. Model-Test Setup and Methodology

The model was connected to the towing carriage by a lightweight wire, one spring, one force sensor, and a seakeeping guiding arm system. The spring stiffness was selected to avoid large initial surge motion amplitudes and surge resonance couplings. Specifically, the eigenfrequency of the arms–model–spring system in the surge direction was smaller than one-half of the lowest wave encounter frequency, as recommended by the International Towing Tank Conference (ITTC) [65]. The resistance was measured with a load cell (Z6 bending beam load cell) directly attached to the carriage through a calibrated pulley–spring–wire system. This setup also included a clamp that holds the model during the acceleration or deceleration phases of the carriage. The seakeeping guiding arm system allowed the model to pitch, heave, and surge (sway, yaw, and roll motions were restrained). Figure 2 presents a schematic of the setup described above.

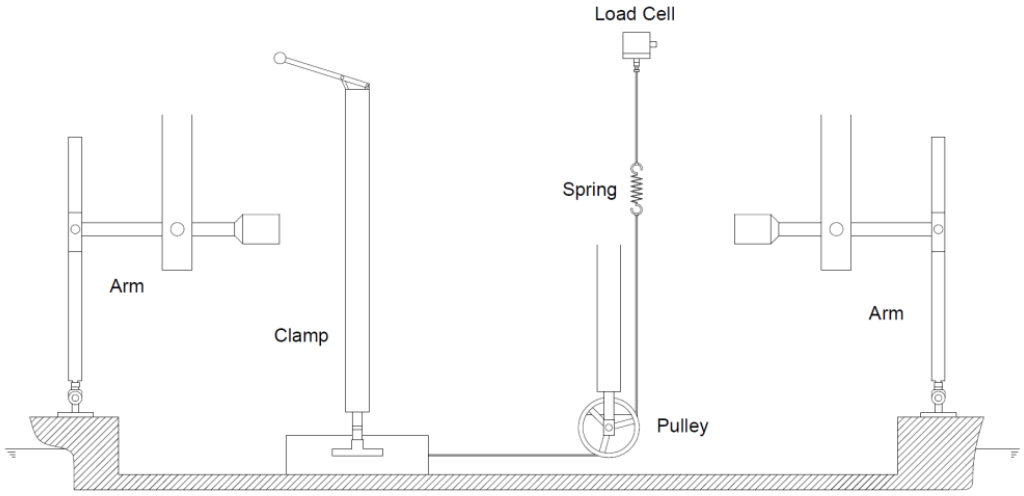

Figure 2. Towing tests setup sketch.

The test methodology followed for each run was kept during the entire campaign. Before each test, the zero reading of all measuring equipment was established over a long enough time. The zero reading was also checked between the runs to avoid zero-drifting-related problems. Since the model was 3D printed, it was continually checked for water intake. The location of the wave probes was decided to obtain fully formed waves and reduce as much as possible the influence of the model and reflected waves on the measurements. Precisely, two wave probes were attached to the carriage (approximately at the aft and forward perpendiculars), and one was located at roughly (3· L of maximum wavelength) m in front of the wavemaker. The wavemaker flap motion was also recorded. As required by ITTC [66], the measured variation in the regular wave height was lower than 5% between the different wave probe positions. The water level was also frequently fixed at the above-mentioned water depth. The model's motions were logged with three AcuRange 500 Laser Position Sensors (AR500). The AR500 is a laser-based triangulation

sensor that records distances by projecting a beam of light onto the target to be measured. The distance was computed from the image pixel data using a microprocessor. Two vertical lasers are able to record the vertical movements, and one longitudinal laser logs the surge motions. The combination of the three gives the pitch rotation motions. All the waves were calibrated without the presence of the model. Possible interference effects caused by the waves reflected by the towing tank side walls were determined by following the method recommended by ITTC for head waves [65]. The maximum value of $F_R.\omega_e\sqrt{L_M/g}$ (F_R is the Froude number, ω_e is encounter wave frequency, L_M is the model length, and g is the gravitational accelerations) at which side-wall interference occurs in head waves (0.314) was always lower than the actual values (0.339–1.307). Figure 3 shows the maximum and minimum $F_R.\omega_e\sqrt{L_M/g}$ for each ship speed compared to the recommended ITTC limits for side-wall interference.

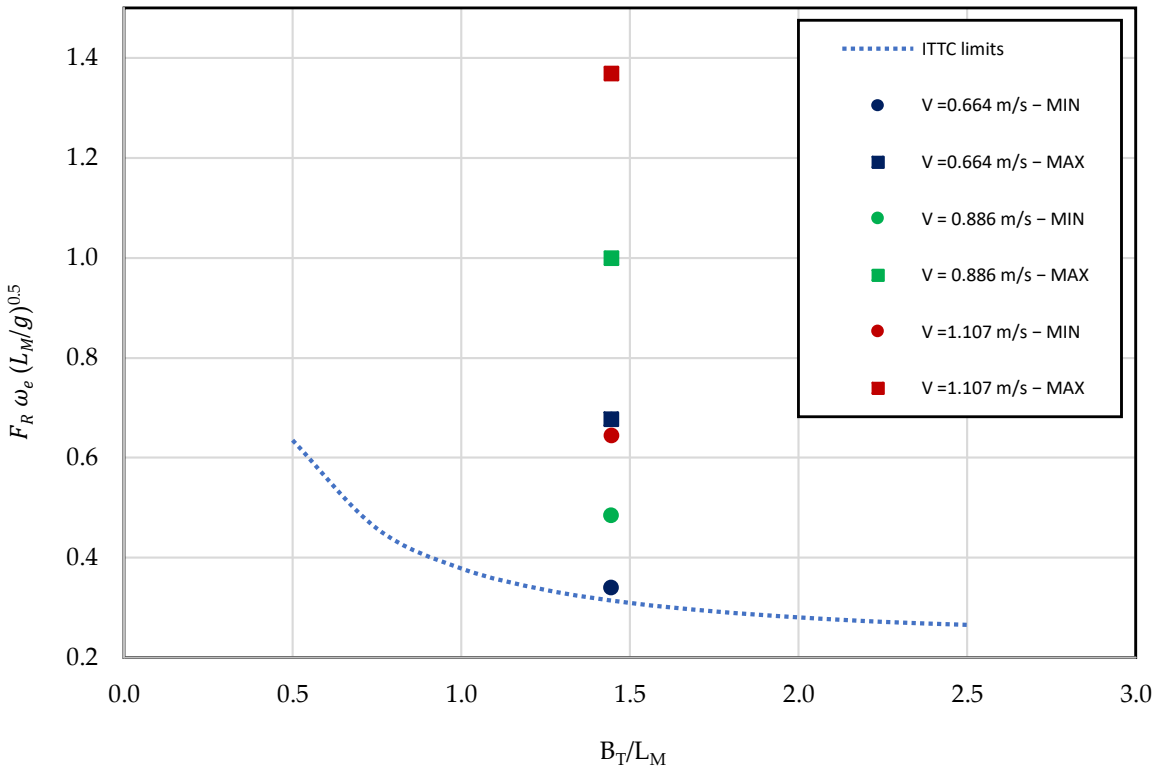

Figure 3. Maximum and minimum values of $F_R.\omega_e\sqrt{L_M/g}$ for each ship speed compared to the recommended ITTC limits for side-wall interference.

4. Uncertainties

The precision errors e_s and $\tilde{e}_s$ (defined in Equation (1)) were used to calculate the repeatability uncertainty for the calm water resistance R_C and the added resistance in waves R_{AW}. The two-tailed Student's t-distribution with $N-1$ degrees of freedom was calculated with a cumulative probability of 0.95. The uncertainties were estimated based on five repeated measurements (as in [67]).

$$e_s = \frac{t_s \cdot S_X}{\bar{M}} \qquad \tilde{e}_s = \frac{t_s \cdot S_X}{\sqrt{N} \cdot \bar{M}} \tag{1}$$

where $\bar{M}$ is the average value of the N repetitions, t_s is Student's t-distribution, and S_X is the standard deviation.

Two representative cases were selected for the uncertainty analysis:

- C_1: calm water conditions with a model speed of 1.107 m/s.

- C_2: regular waves with a model speed of 1.107 m/s, wave height of 0.057 m, and wave period of 1.298 s.

Table 3 shows the uncertainties for e_s and $\tilde{e}_s$ for the two cases. It is possible to notice that the uncertainties are higher in waves than in calm water conditions, as reported also by Saettone et al. [67]. The uncertainty analysis results align with the standard measurement error range for calm water and added resistance in waves, as presented by Saettone et al. [48].

Table 3. Uncertainties.

Case		v [m/s]	λ_w/L_{PP} [-]	T_w [s]	e_s [%]	$\tilde{e}_s$ [%]
C_1	R_C	1.107	—-	—	0.91	0.41
C_2	R_{AW}	1.107	1.000	1.298	2.68	1.20

The regular waves generated during the tests indicated that the wave elevations were not completely stationary even under steady-state conditions but contained small fluctuations during the different cycles. On the other hand, the regular wave frequency was remarkably stable. Therefore, the wave elevation characteristics were analysed for a minimum of 20 cycles to reveal variations in the regular wave tests and wave probe sensitivity.

5. Computational Strategy

5.1. Mathematical Model

Numerical simulations were performed using SHIPFLOW MOTIONS (version 7) [68], a time-dependent potential flow solver. The main advantage of such a solver is the low computational cost combined with accurate results, as proven in other studies (e.g., [69,70]).

The numerical simulations were based on the potential flow theory [26]. The flow is assumed to be nonviscous, incompressible, and irrotational based on the potential flow assumption. As a result, in the fluid zone, there exists a velocity potential function that fulfills the Laplace equation.

$$\nabla^2 \varnothing = 0 \tag{2}$$

The velocity potential on the free surface satisfies the kinematic and dynamic boundary conditions.

$$\frac{D\varnothing}{Dt} = -\nabla\varnothing \tag{3}$$

$$\frac{D\varnothing}{Dt} = -gz + \frac{1}{2}\nabla\varnothing\cdot\nabla\varnothing - \frac{P_a}{\rho} \tag{4}$$

where $\vec{x} = (x, y, z)$ is the coordinates of the free surface, and P_a is the atmospheric pressure.

An impermeable boundary condition is used on the hull surface, as it follows:

$$\frac{\partial\varnothing}{\partial n} = \vec{n}\cdot(\vec{u} + \vec{\omega}\times\vec{\gamma}') \tag{5}$$

where $\vec{n}$ is the vertical component of the hull surface, $\vec{u}$ and $\vec{\omega}$ are the linear velocity and angular velocity, and $\vec{\gamma}'$ is the radial velocity of the rotation centre.

Any location in the computational domain's unsteady hydrodynamic pressure is solved using the Bernoulli equation:

$$p = -\rho\left(\frac{\partial\varnothing}{\partial t} + \frac{1}{2}|\nabla\varnothing|^2 + gz\right) \tag{6}$$

The partial derivative of the time-dependent velocity potential is:

$$\frac{\partial \varnothing}{\partial t} = \frac{d\varnothing}{dt} - \vec{v}' \nabla \varnothing \tag{7}$$

where $\vec{v}'$ is the velocity of solution point.

Integrating along the wet surface gives the hull's bending moment and hydrodynamic force, i.e.:

$$\vec{F} = -\iint_{S_b} p\vec{n}dS \tag{8}$$

$$\vec{M} = -\iint_{S_b} p(\vec{\gamma}' \times \vec{n})S \tag{9}$$

where, $\vec{F} = (F_x, F_y, F_z)$ and $\vec{M} = (M_x, M_y, M_z)$.

5.2. Grid Convergence Test

Potential flow calculations in SHIPFLOW MOTIONS are performed considering the hull with unit length. When performing numerical simulations, the main source of numerical errors and uncertainties comes from grid discretization, incomplete iterative convergence, and computer round-off. In the current analysis, a verification study was conducted to determine the numerical errors and uncertainties from the grid discretization for the calm water and added resistance in waves. The computer round-off error and the iterative uncertainty were assumed to be negligible. The tested grids had a maximum refinement level on the free surface from 5 to 7, and for the body, a minimum refinement level from 6 to 8. The method used for grid validation is estimating errors and uncertainties with a Correction Factor, which is based on Richardson Extrapolation [71]. The parameter refinement ratio was considered $r_i = \sqrt{2}$. The converge conditions can be estimated as shown in the following equations based on the solutions obtained, where S_1, S_2 *and* S_3 are the solutions obtained.

$$\varepsilon_{32} = S_3 - S_2 \; and \; \varepsilon_{21} = S_2 - S_1 \tag{10}$$

The convergence ratio, R_i, was estimated according to the following equations:

$$R_i = \varepsilon_{21}/\varepsilon_{32} \tag{11}$$

For our case, $0 < R_i < 1$, which means that we are in the case of monotonic convergence. Having three solutions, the estimates for error (δ_{RE}) and order of accuracy (p_i) were calculated as follows:

$$\delta_{RE} = \frac{\varepsilon_{21}}{r_i^{p_i} - 1} \tag{12}$$

$$p_i = \frac{ln(\varepsilon_{31}/\varepsilon_{21})}{ln(r_i)} \tag{13}$$

Regarding the numerical uncertainty, U_i can be estimated according to the observed order of accuracy, and for the case of monotonic convergence:

$$U_i = (|C_i| + \lfloor 1 - C_i \rfloor)|\delta_{RE}| \tag{14}$$

where C_i represent the correction factor.

The result of the numerical uncertainty, U_i, for calm water and for waves are presented in Table 4, and as can be noticed, the percentages are agreeable.

For our study, the finest grid was chosen to investigate the additional wave resistance for the seven wavelengths and three wave heights. The simulations were performed on three computers with four cores of 3.1 GHz, and the total number of cases was 72.

Table 4. Grid convergence test results.

Variable		R_C [N]	R_{AW} [N]
V [m/s]		1.107	1.107
λ_w/L_{PP} [-]		—-	1.000
T_w [s]		—	1.298
No. of panels	S_1 (fine)	2566	6596
	S_2 (medium)	1797	4722
	S_3 (coarse)	1251	3368
ε_{21}		0.003	0.005
ε_{32}		0.026	0.014
r_i		1.2	1.2
R_i		0.12	0.35
p_i		11.84	5.64
δ_{RE}		0.00391	0.00277
U_i [%]		2.02	3.16

6. Analysis of the Results

6.1. Resistance in Still Water

The primary objective of the calm water tests is to establish the resistance curve used to estimate the added resistance in waves. The resistance curve was also compared to the experimental results published by El Moctar et al. [64]. However, since the scale factor of model used by El Moctar is 1:59.407, different to the scale used in the present study (1:135), the measurements were extrapolated based on the ITTC 57 method to allow for a proper comparison. On the other hand, the numerical simulations were performed at the same scale as for the experimental tests conducted at ETSIN-UPM; therefore, no extrapolation was needed to compare the EFD and CFD results obtained during the present investigations.

The two resistance curves, displayed in Figure 4 (where the EFD results are from the experimental test performed at ETSIN-UPM and the SVA Postdam are the results from the benchmark), show a satisfactory comparison. Numerical simulations were also performed, and the results were added to Figure 3. The CFD resistance curve shows a good comparison with the UPM experimental data. It is also important to note that during the calm water tests, no non-stationary effects were observed based on the qualitative analysis of Figure 5.

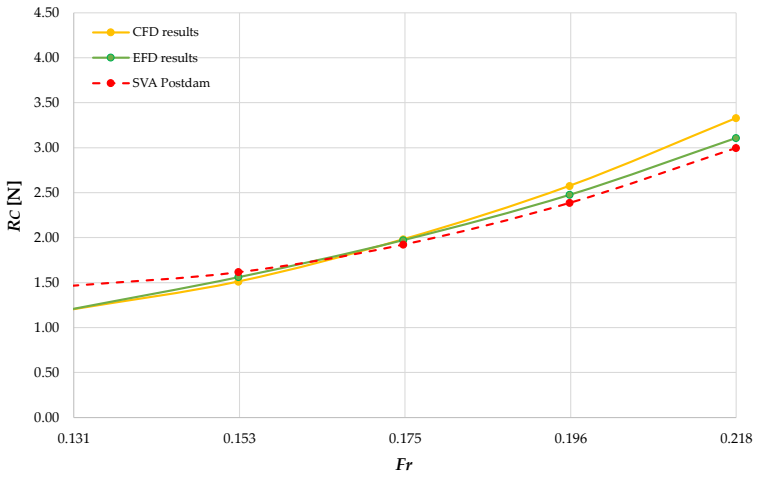

Figure 4. Resistance test.

(**a**) (**b**) (**c**)

Figure 5. Calm water resistance: (**a**) $F_R = 0.131$; (**b**) $F_R = 0.174$; (**c**) $F_R = 0.218$.

6.2. Wave-Added Resistance

The added resistance coefficient, pitch RAO, and heave RAO were computed. The added resistance coefficient was calculated as follows:

$$C_{AW} = \frac{R_{Tw} - R_C}{\rho \cdot g \cdot (H_w/2)^2 \cdot B_{WL}^2 / L_{PP}} = \frac{R_{AW}}{\rho \cdot g \cdot (H_w/2)^2 \cdot B_{WL}^2 / L_{PP}} \quad (15)$$

where R_{Tw} is the total resistance in waves, R_C is the total resistance in calm water, ρ is the density of the water, g is the gravitational acceleration, H_w is the wave height, B_{WL} is the waterline beam of the model, and L_{PP} is the length between perpendiculars. The response amplitude operators for heave and pitch were calculated to examine the ship's behaviour in regular waves.

Overall, 21 cases were tested: seven wavelengths in a range of λ_w/L_{PP} from 0.5 to 1.5 and three wave heights, H_w of 0.03 m, 0.044 m, and 0.057 m. Furthermore, three different model speeds, 0.664, 0.885 and 1.107 m/s, corresponding to Froude numbers of 0.13, 0.17 and 0.22, were tested for each of the above cases. The added resistance in waves and heave and pitch RAOs at different wave amplitudes for the lowest speed are presented in Figure 6.

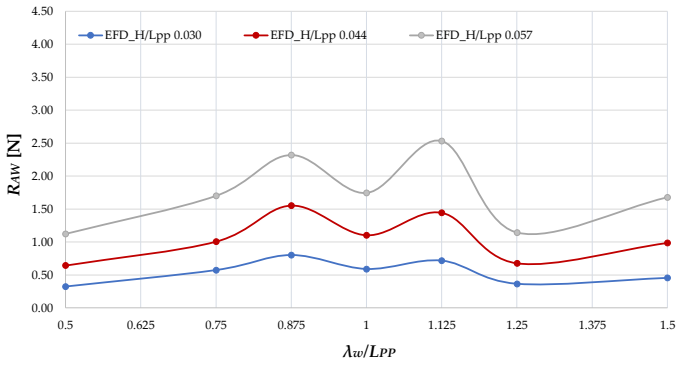

(**a**)

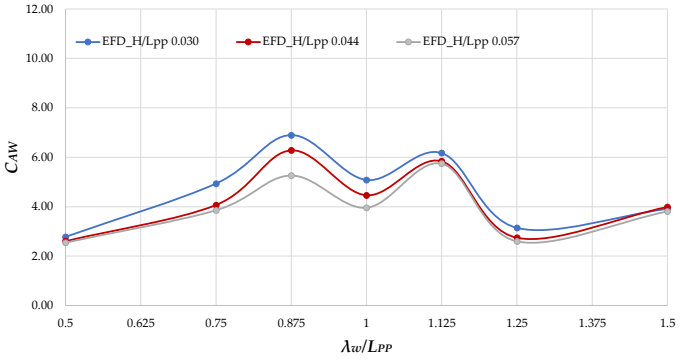

(**b**)

Figure 6. *Cont.*

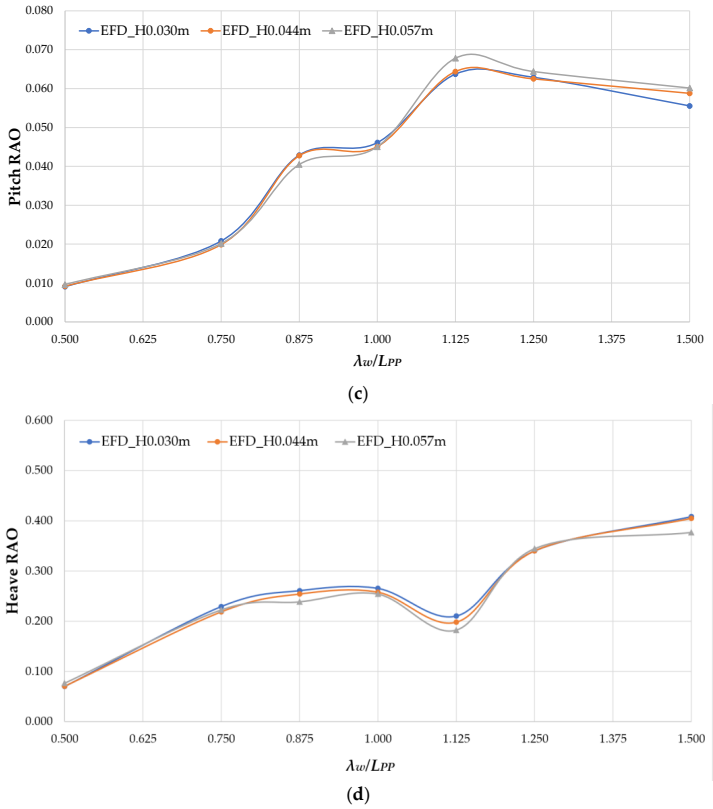

Figure 6. EFD results for the lowest speed corresponding to $F_R = 0.131$: (**a**) added resistance in waves; (**b**) added resistance coefficient; (**c**) Pitch RAO; (**d**) Heave RAO.

Usually, the added resistance curve has only one peak where the wavelength is approximately equal to the ship length. However, for the lowest ship speed, the curve shows two local maxima: one at $\lambda_w/L_{PP} = 0.875$ and the other at 1.125. This trend is consistent for all the wave heights, as shown in Figure 6a. It is also possible to notice that the double resonance phenomena are more significant with the increase in wave steepness. On the contrary, only one peak value can be seen for the higher ship speeds, as shown in Figure 7. The pitch motions presented in Figure 6c show a good correlation between the pitch curve and non-dimensionalised added resistance in waves. Two local maxima corresponding to $\lambda_w/L_{PP} = 0.875$ and $\lambda_w/L_{PP} = 1.125$ also appear on the pitch curve. The heave RAO curves for the lowest speed drop significantly at $\lambda_w/L_{PP} = 1.125$. However, no heave drop can be noticed for the wavelength of $\lambda_w/L_{PP} = 0.875$. This may suggest that the unexpected increase in added resistance coefficient could be related to increased pitch motions. In addition, it is also possible to see that wave amplitude has a small influence on the heave and pitch RAOs. Another observation that can be made is related to wave steepness. Increasing the steepness does not affect the double resonance phenomena, and the only thing that changes is the migration of the absolute maximum from $\lambda_w/L_{PP} = 0.875$ at lower steepness to the $\lambda_w/L_{PP} = 1.125$ at highest steepness.

Considering the abovementioned findings, calculations have been made based on different linear prediction approaches implemented in the commercial software NAPA 2022.2. Linear methods based on the far-field method of Gerritsma and Beukelman [7] and the near-field Faltinsen method [11] were employed. An empirical method based on the work of Liu and Papanikolaou [72] was also utilised. Comparisons of the results obtained with the abovementioned methods, the non-linear 3D Rankine method (SHIPFLOW), and experimental measurements in terms of added resistance in waves are presented in Figure 6 for three different speeds at the lowest wave height. Neither linear nor non-linear panel methods could capture the double peak behaviour in the experiment measurements at the lowest speed. Consequently, this should be related to the strongly non-linear phenomena.

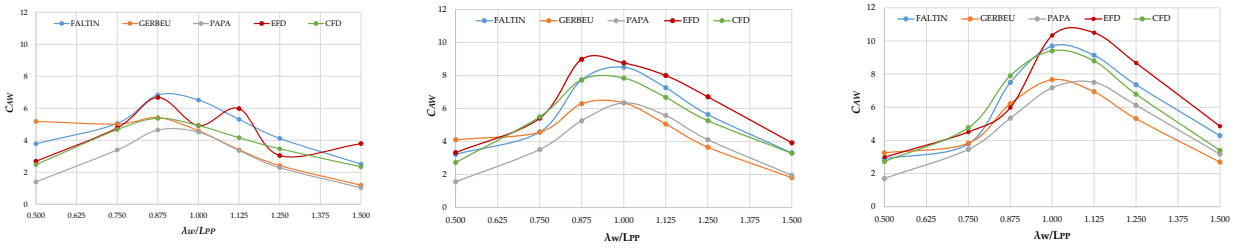

(**a**) (**b**) (**c**)

Figure 7. Comparisons of the results for added resistance coefficient: (**a**) $F_R = 0.131$; (**b**) $F_R = 0.174$; (**c**) $F_R = 0.218$.

A more in-depth analysis was carried out considering the 3D fully non-linear time-domain-based Rankine panel method. The numerical analysis followed the same cases as in the model testing conducted in the towing tank. The results for each speed and the comparison between the experimental test and numerical simulations are presented in Figure 8. The double resonance phenomena found during the experimental tests were not captured by the potential flow panel method. However, the non-dimensional amplitudes of heave and pitch and the added resistance coefficient decrease as wave steepness increases, as observed in both the computational and experimental results.

The agreement between the calculations and experiments is satisfactory, indicating that the CFD method utilized in this study can accurately predict ship motions and total resistance, effectively accounting for the influence of wave steepness, except for the double resonance phenomenon. The percentage error was calculated as shown in the following equation to evaluate the difference between the experimental results and the numerical simulations.

$$PE = \frac{\left| R_{T_{EFD}} - R_{T_{CFD}} \right|}{R_{T_{EFD}}} \cdot 100\ [\%] \tag{16}$$

Table 5 shows the error percentages in the case of total resistance for the highest speed, corresponding to $F_R = 0.218$, and wave height, H_w of 0.03 m.

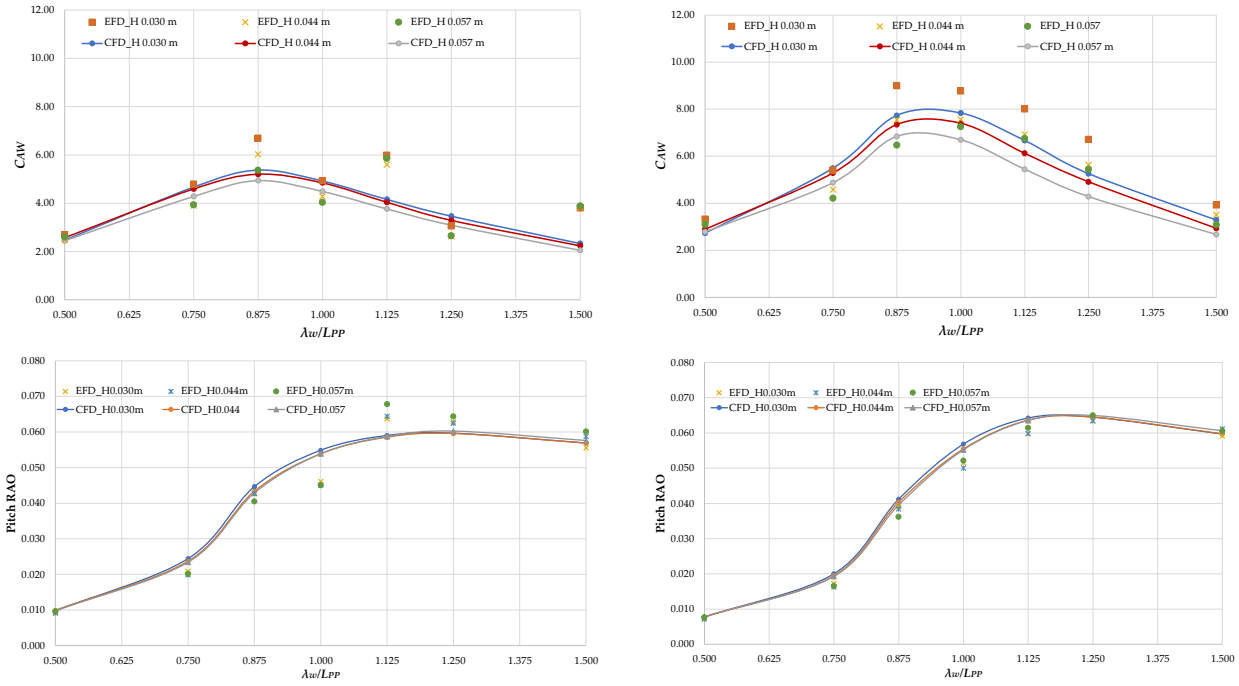

Figure 8. *Cont.*

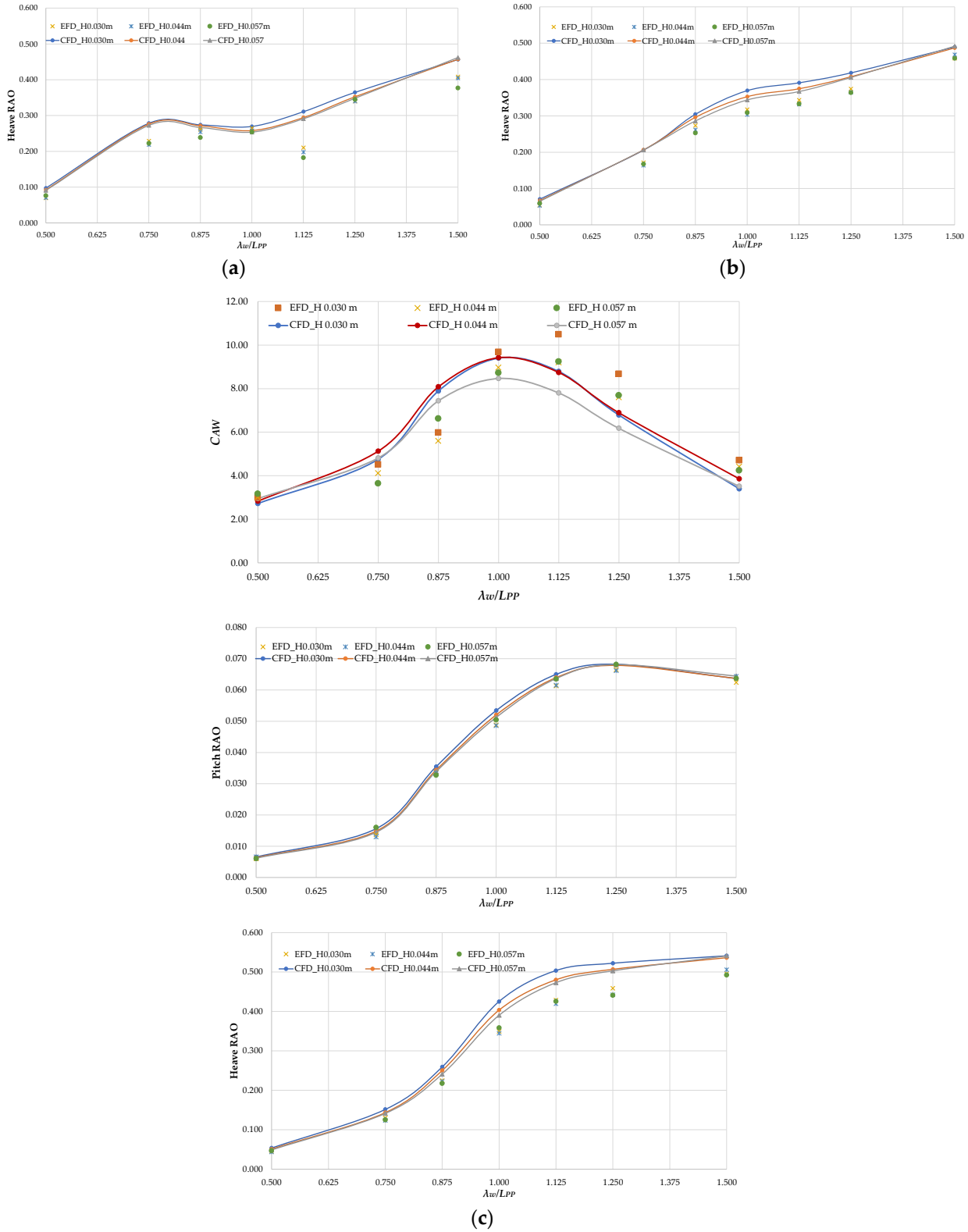

Figure 8. EFD and CFD Results for: (**a**) $F_R = 0.131$; (**b**) $F_R = 0.174$; (**c**) $F_R = 0.218$.

Table 5. Percentage error.

		F_R = 0.131	F_R = 0.174	F_R = 0.218
H_w [m]	λ_w/L_{PP}		PE[%]	
0.030	0.500	1.921	2.804	2.91
	0.750	0.311	1.279	1.66
	0.875	5.885	5.569	5.00
	1.000	0.823	2.626	0.66
	1.125	11.533	4.649	2.92
	1.250	1.873	6.466	4.10
	1.500	12.514	5.119	4.06
0.044	0.500	2.335	4.141	3.59
	0.750	4.424	0.617	0.61
	0.875	8.979	5.041	7.68
	1.000	2.283	2.273	0.26
	1.125	18.300	5.421	2.58
	1.250	4.167	7.533	3.93
	1.500	23.536	7.226	5.36
0.057	0.500	5.792	6.017	3.53
	0.750	0.354	2.165	4.38
	0.875	6.319	1.126	0.35
	1.000	4.445	1.524	0.80
	1.125	26.531	7.110	3.02
	1.250	2.788	10.183	5.69
	1.500	33.186	7.942	6.70

To further investigate the double peak phenomena, a comparison of the wave elevation in the bow area of the experimental tests and numerical simulations for the lowest speed (F_R = 0.131) and lowest wave height (0.030) was conducted (see Figure 9). The comparisons revealed that the bow wave observed during the experiment was characterized by lower strength overturning when the bow reached the maximum immersion, which cannot be captured by the potential flow method. Otherwise, the wave elevation in the bow area seemed to be similar.

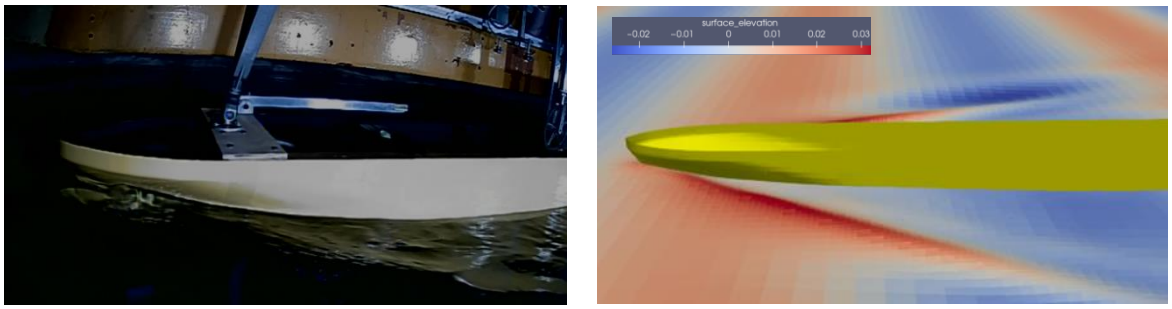

Figure 9. *Cont.*

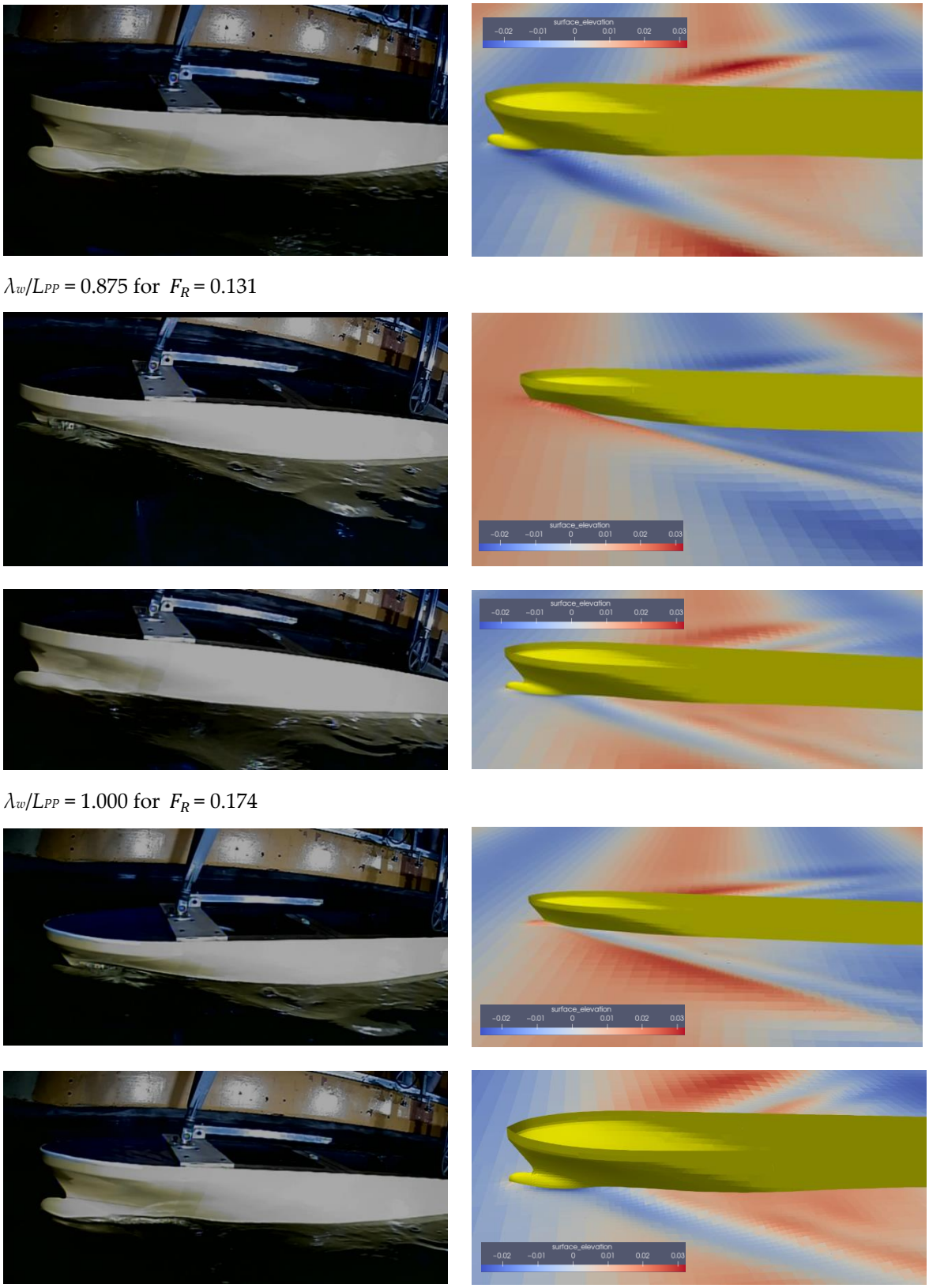

λ_w/L_{PP} = 0.875 for F_R = 0.131

λ_w/L_{PP} = 1.000 for F_R = 0.174

λ_w/L_{PP} = 1.125 for F_R = 0.218

Figure 9. Wave elevation comparison between the experimental tests and numerical simulations.

Another phenomenon that can affect the added resistance is the nonlinear behaviour of the bow wave [52]. Choi and Huijsmans [73] and Huijsmans and Wellens [74] investigated the nonlinearity of added resistance induced by bow wave breaking. To study this aspect, they made visual observations during the experimental test in regular head waves, and three categories were identified: plunging breakers, spilling breakers, and non-breaking conditions. Plunging is defined as an overturning detachment of the bow wave crest, and spilling is a type of turbulent form that disturbs the adjacent flow field [73]. Therefore, a similar qualitative analysis of the bow wave recorded during the tests was conducted to determine whether the double peak found on the added resistance coefficient curve could be related to the change in type or the strength of bow wave breaking. After a systematic analysis of all recordings made during the experiments, it can be concluded that no significant change of the bow wave can prove the drop of the added resistance in waves at λ_w/L_{PP} equal to 1.0, as shown in Figure 10. For the highest wave height at λ_w/L_{PP} equal to 1.125, one can notice a supplementary immersion of the bow in comparison with the other two wavelength cases (Figure 9) and slightly green water that can justify the increase in the added resistance in waves higher than the first peak at λ_w/L_{PP} equal with 0.825 (Figure 8).

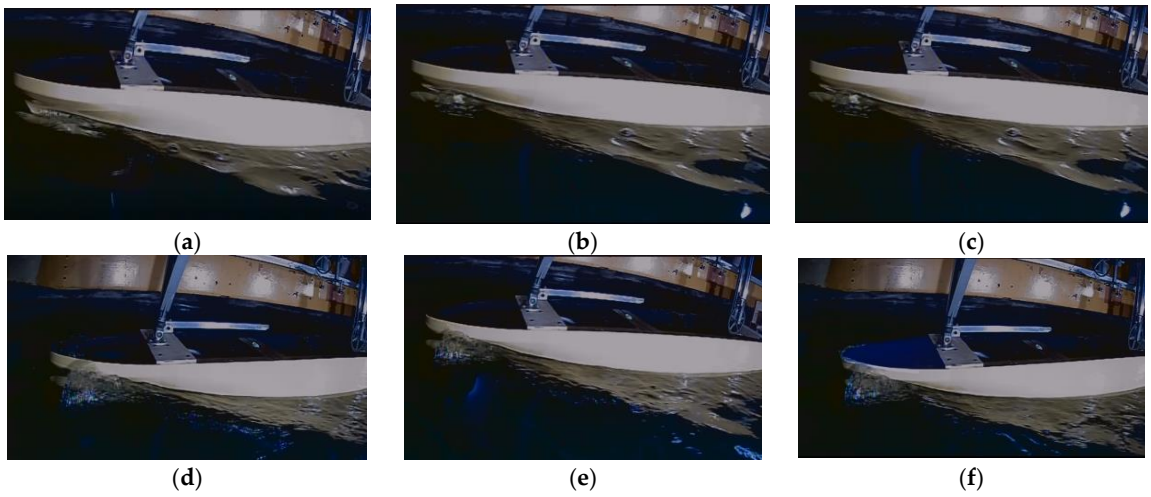

Figure 10. Flow around hull for the following cases: (**a**) λ_w/L_{PP} = 0.875 for F_R = 0.131 and H_w = 0.03 m; (**b**) λ_w/L_{PP} = 1.000 for F_R= 0.131 and H_w = 0.03 m; (**c**) λ_w/L_{PP} = 1.125 for F_R= 0.131 and H_w = 0.03 m; (**d**) λ_w/L_{PP} = 0.875 for F_R= 0.131 and H_w = 0.057 m; (**e**) λ_w/L_{PP} = 1.000 for F_R= 0.131 and H_w = 0.057 m; (**f**) λ_w/L_{PP} = 1.125 for 0.664 m/s and H_w = 0.057 m.

On the other hand, the variation in model speed, wavelength, and wave height might lead to different interference conditions of the wave-making and incident waves. This, combined with the hydrodynamic nonlinearities due to model geometry, might create a wide range of harmonics with several resonance peaks. Also contributing to this phenomenon are the various changes in the free surface conditions caused by the nonlinear interactions of the head waves and eigenwaves. This might lead to changes in the natural frequency of the model.

6.3. Non-Quadratic Correlation of Added Resistance Coefficient

As previously mentioned, the added resistance is a second-order phenomenon, and the magnitude of the added resistance is considered, based on the linear theory, proportional to the square of the wave amplitude [7,75].

In other words, the added resistance coefficient should be constant for different wave amplitudes. However, as seen in Figure 8, the numerically computed and experimentally measured curves of the dimensionless added resistance do not coincide for the three wave amplitudes. Consequently, the added resistance in waves, for the cases studies, is not proportional to the square of the wave amplitude. This result is in line with the

recent investigations carried out on the effect of steepness on the added resistance in waves [26,52,57,58,76,77].

A deeper investigation was performed into the power relationship between wave height and added resistance. A power of 1.75 instead of 2 was found to provide the best match between wave height and added resistance in waves. This result is consistent for both the non-linear 3D Rankine method implemented in SHIPFLOW and the experiments. Figure 11 shows the added resistance coefficient, determined experimentally, against the wave steepness using the power of 2 and 1.75 for the wave height. Figure 12 shows the same type of plot with the added resistance coefficient computed with SHIPFLOW.

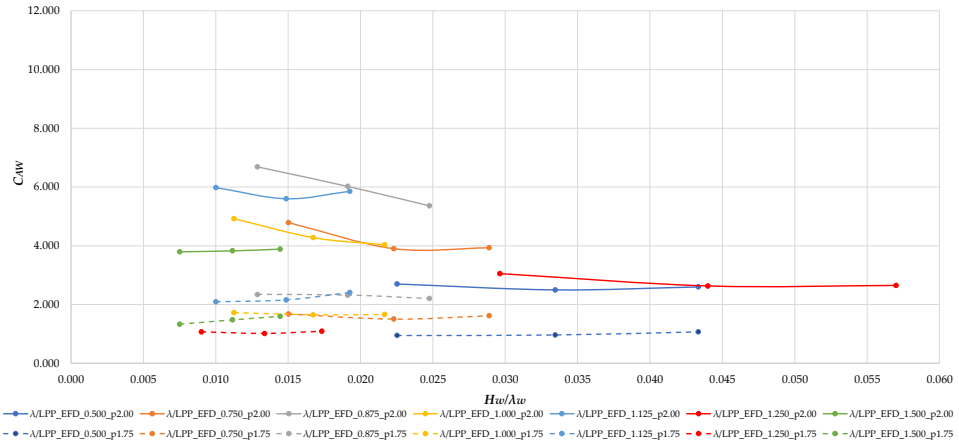

(**a**)

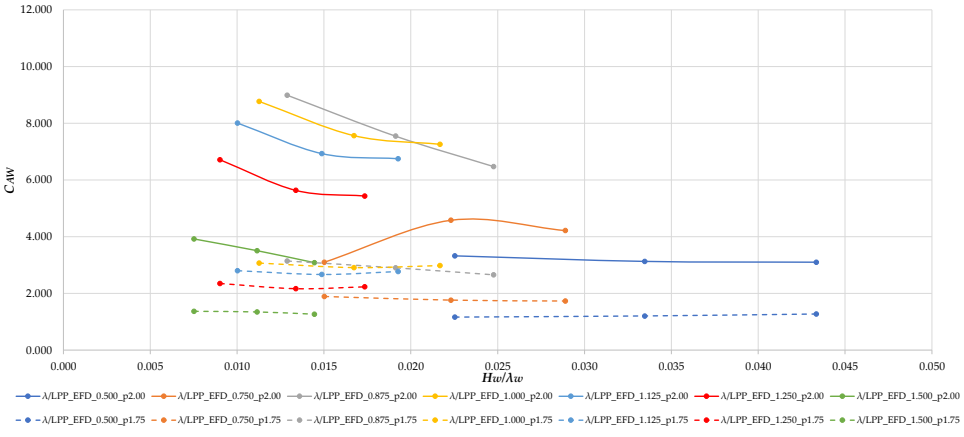

(**b**)

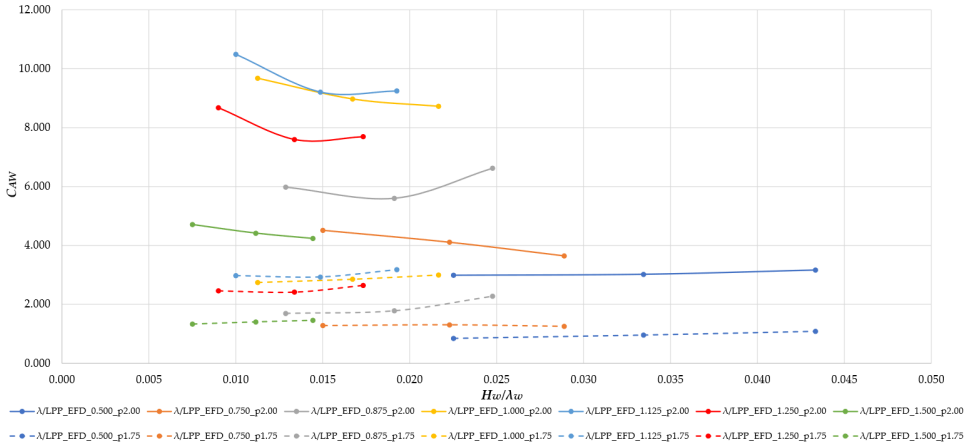

(**c**)

Figure 11. EFD results, steepness effect for each speed: (**a**) $F_R = 0.131$; (**b**) $F_R = 0.174$; (**c**) $F_R = 0.218$.

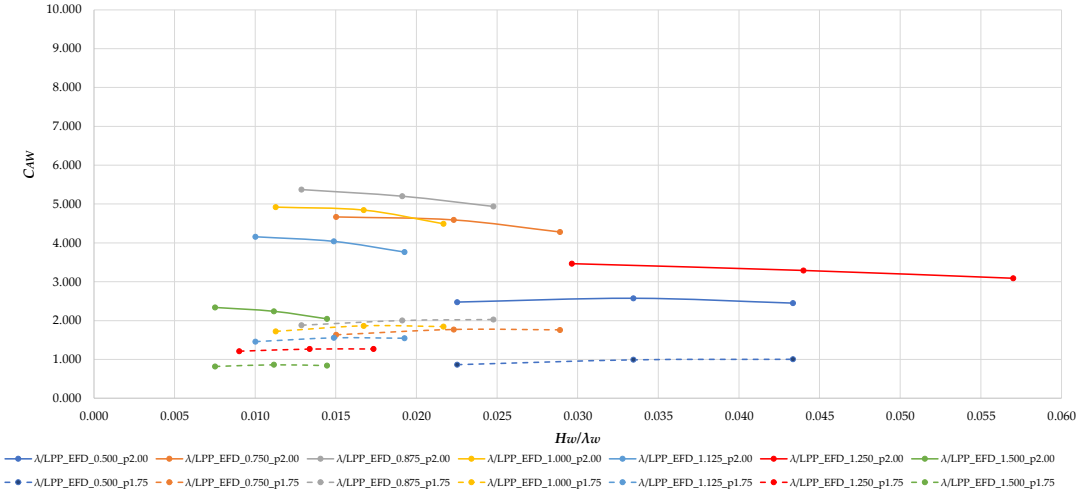

(**a**)

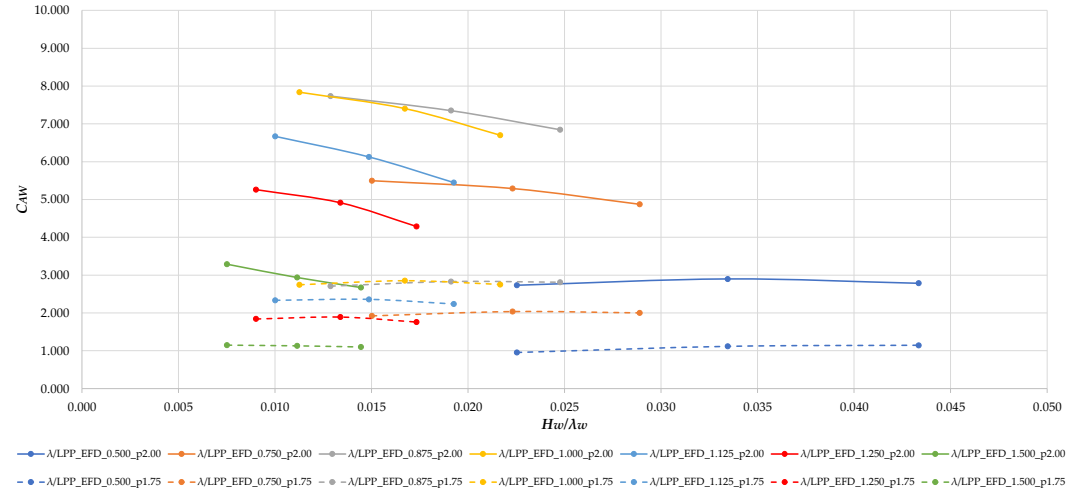

(**b**)

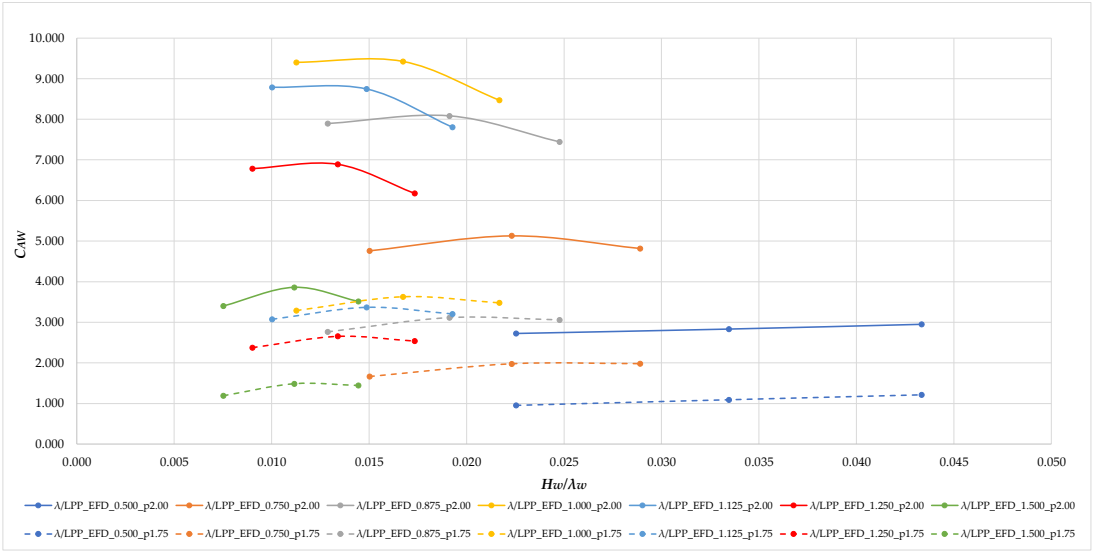

(**c**)

Figure 12. CFD results, steepness effect for each speed: (**a**) $F_R = 0.131$; (**b**) $F_R = 0.174$; (**c**) $F_R = 0.218$.

7. Conclusions

In the present paper, experimental and numerical methods were employed to determine the added resistance in regular head waves of the DTC hull with a scale factor of 135. Three Froude numbers (0.13, 0.17, and 0.22), seven wavelengths (λ_w/L_{PP} = 0.500, λ_w/L_{PP} = 0.750, λ_w/L_{PP} = 0.875, λ_w/L_{PP} = 1.000, λ_w/L_{PP} = 1.125, λ_w/L_{PP} = 1.250, and λ_w/L_{PP} = 1.500), and three wave heights (0.030, 0.044, and 0.057 m) were considered.

The results proved that the effectiveness of the linear theory in predicting the added resistance in waves might be limited since the commonly used added resistance coefficient reduces with the increase in wave steepness. Changing the power of the wave amplitude to 1.75 (instead of 2) in the added resistance coefficient determined experimentally provided the best match between wave height and added resistance in waves. This result was also valid for the added resistance coefficient computed with the non-linear 3D Rankine method implemented in SHIPFLOW. This demonstrates that the potential flow theory can predict this phenomenon accurately.

Furthermore, an unexpected double resonance effect on the added resistance curve was found at V = 0.664 m/s and corresponded to a Froude number of 0.13. In this case, the added resistance curve showed two local maxima, one at λ_w/L_{PP} = 0.875 and the other at λ_w/L_{PP} = 1.125, that increased with the wave steepness. An in-depth systematic analysis of the recordings made during the experiments led to the conclusion that no significant change of the bow wave could prove the drop of the added resistance in waves at λ_w/L_{PP} = 1.0.

The results also revealed a generally acceptable agreement between the 3D fully non-linear time-domain-based Rankine panel method and experiments, except for the double resonance phenomenon that occurred for the lowest speed investigated.

The primary limitation of this type of research approach is the issue of generalizing the results. Thus, the need for future work in terms of investigating more cases is undeniable. Moreover, a more in-depth analysis of the causes of the double resonance phenomenon for the DTC is required. Specifically, additional towing tank tests must be carried out for different ship speeds and wave characteristics. Finally, unsteady RANS computations will also be performed to obtain a better comparison with the experimental data.

Author Contributions: Conceptualization A.-M.C., A.M., F.P. and S.S.; methodology F.P., S.S., L.R. and S.P.; towing tests S.S., A.M., A.-M.C., F.P. and S.P.; software simulations, validation, analysis, and visualization A.-M.C. and F.P.; writing—original draft preparation A.-M.C., S.S. and F.P.; supervision and writing final version, F.P., S.S., L.R. and S.P. All authors have read and agreed to the published version of the manuscript.

Funding: This work was carried out in the framework of the research project CLIMEWAR (CLimate change IMpact Evaluation on future WAve conditions at Regional scale for the Black and Mediterranean seas marine system), supported by the Romanian Executive Agency for Higher Education, Research, Development and Innovation Funding—UEFISCDI, grant number PN-III-P4-PCE-2021-0015.

Institutional Review Board Statement: Not applicable.

Informed Consent Statement: Not applicable.

Data Availability Statement: Not applicable.

Conflicts of Interest: The authors declare no conflict of interest.

Nomenclature and Definitions

Terms

B_{WL}	Waterline breadth
C_{aw}	Added resistance coefficient
c_B	Block coefficient
F_R	Froude number
g	Gravitational accelerations

H_w	Wave height
L_M	Model length
L_{PP}	Length between perpendiculars
PE	Percentage error
RAO	Response Amplitude Operator
R_{AW}	Added resistance in waves
R_C	Calm water resistance
R_{Tw}	Total resistance in waves
$R_{T_{CFD}}$	Total resistance for numerical simulations
$R_{T_{EFD}}$	Total resistance for experimental tests
ryy	Radius of gyration
S_w	Wetted surface
T	Draught midship
T_w	Wave period
V	Speed
ω_e	Encounter wave frequency
X_{CB}	Longitudinal centre of buoyancy measured from the transom
X_{CB}	Longitudinal centre of buoyancy—from aft perpendicular
X_{CF}	Longitudinal centre of flotation—measured the from transom
X_{CG}	Longitudinal centre of gravity—from aft perpendicular
Z_{CB}	Vertical centre of buoyancy—from baseline
Z_{CG}	Vertical centre of gravity—from aft perpendicular
λ	Scale
λ_w	Wave length
∇	Volume displacement
ρ	Water density
Abbreviation	
AR500	AcuRange 500 Laser Position Sensors
BEM	Boundary element method
CFD	Computational fluid dynamics
DTC	Duisburg Test Case
CII	Carbon Intensity Indicator
EEDI	Energy Efficiency Design Index
EEXI	Energy Efficiency Existing Ship Index
EFD	Experimental fluid dynamics
ETSIN-UPM	Escuela Técnica Superior de Ingeniería de Montes, Universidad Politécnica de Madrid
IGES	Initial Graphics Exchange Specification
IMO	International Maritime Organization
ITTC	International Towing Tank Conference
JBC	Japan Bulk Carrier
PLA	Polylactic Acid
NAPA	Naval Architectural Package (Software Package)
QTF	Quadratic transfer function
RANS	Reynolds-averaged Navier–Stokes equation
VOF	Volume of fluid

References

1. Gao, Q.; Song, L.; Yao, J. RANS Prediction of Wave-Induced Ship Motions, and Steady Wave Forces and Moments in Regular Waves. *J. Mar. Sci. Eng.* **2021**, *9*, 1459. [CrossRef]
2. Havelock, T.H. The Resistance of a Ship among Waves. *Proc. R. Soc. Lond. A* **1937**, *161*, 299–308.
3. Maruo, H. The excess resistance of a ship in rough seas. *Int. Shipbuild. Prog.* **1957**, *4*, 337–345. [CrossRef]
4. Maruo, H. The drift of a body floating on waves. *J. Ship Res.* **1960**, *4*, 51–60.
5. Maruo, H. Resistance in waves. In *60th anniversary Series*; The Society of Naval Architects of Japan: Tokyo, Japan, 1963; Volume 8, pp. 67–102.
6. Joosen, W.P.A. Added resistance of ships in waves. In Proceedings of the 6th Symposium on Naval Hydrodynamics, Washington, DC, USA, 18 September–4 October 1966; p. 637.

7. Gerritsma, J.; Beukelman, W. Analysis of the resistance increase in waves of a fast cargo ship. *Int. Shipbuild. Prog.* **1972**, *19*, 285–293. [CrossRef]
8. Salvesen, N. Second-order steady state forces and moments on surface ships in oblique regular waves. In *International Symposium on Dynamics of Marine Vehicles and Structures in Waves*; University College: London, UK, 1974; Paper 22; pp. 225–241.
9. Korvin-Kroukovsky, B.V.; Jaeobs, W.R. Pitching and Heaving Motions of a Ship in Regular Waves. *Trans. Sname* **1957**, *65*, 590–632.
10. Boese, P. Eine einfache methode zur berechnung der widerstandserhöhung eines schiffes im seegang. *Schr. Schiffbau* **1970**, *258*, 1–9. [CrossRef]
11. Faltinsen, O.M.; Minsaas, K.J.; Liapis, N.; Skjordal, S.O. Prediction of resistance and propulsion of a ship in a seaway. In *3th Symposium on Naval Hydrodynamics*; Sasakawa Hall: Tokyo, Japan; ONR: Arlington, VA, USA, 1980.
12. Newman, J.N. *Marine Hydrodynamics*, 1st ed.; MIT Press: Cambridge, MA, USA, 1977.
13. Faltinsen, O.M. *Hydrodynamics of High-Speed Marine Vehicles*; Cambridge University Press: Cambridge, UK, 2005.
14. Belga, F.; Sutulo, S. Guedes Soares. Comparative study of various strip-theory seakeeping codes in predicting heave and pitch motions of fast displacement ships in head seas. In *Progress in Maritime Engineering and Technology*; CRC Press: Boca Raton, FL, USA, 2018.
15. Gasparotti, C.; Domnisoru, L.; Popescu, G.; Amoraritei, M. Maritime operation safety assessment, using seakeeping criteria, of an offshore barge in the Caspian Sea. 16th International Multidisciplinary Scientific GeoConference SGEM, Albena, Bulgaria, 30 June–6 July 2016; Volume 16, Book 1, Part 1. pp. 783–790, ISBN 978-1-5108-2990-9.
16. Rusu, L.; Guedes Soares, C. Forecasting fishing vessel responses in coastal areas. *J. Mar. Sci. Technol.* **2014**, *19*, 215–227. [CrossRef]
17. Amini-Afshar, M. Salvesen's Method for Added Resistance Revisited. *J. Offshore Mech. Arct. Eng.* **2021**, *143*, 051902. [CrossRef]
18. Ye, H.K.; Hsiung, C.C. Computation of added wave resistance of a restrained floating body in the time-domain. *Int. Shipbuild. Prog.* **1997**, *44*, 25–57.
19. Choi, Y.R.; Hong, S.Y.; Choi, H.S. An analysis of second-order wave forces on floating bodies by using a higher-order boundary element method. *Ocean Eng.* **2000**, *28*, 117–138. [CrossRef]
20. Fang, M.C.; Chen, G.R. On the nonlinear hydrodynamic forces for a ship advancing in waves. *Ocean Eng.* **2006**, *33*, 2119–2134. [CrossRef]
21. Joncquez, S.A.G.; Bingham, H.; Andersen, P. Validation of added resistance computations by a potential flow boundary element method. In Proceedings of the 27th Symposium on Naval Hydrodynamics, Seoul, Republic of Korea, 5–10 October 2008.
22. Kim, K.H.; Kim, Y. Numerical study on added resistance of ships by using a time domain Rankine panel method. *Ocean Eng.* **2011**, *38*, 1357–1367. [CrossRef]
23. Soding, H.; Shigunov, V.; Schellin, T.E.; El Moctar, O. A Rankine Panel Method for Added Resistance of Ships in Waves. *ASME J. Offshore Mech. Arct. Eng.* **2014**, *136*, 031601. [CrossRef]
24. Zhang, W.; Moctar, O.E. Numerical prediction of wave added resistance using a Rankine Panel method. *Ocean Eng.* **2019**, *178*, 66–79. [CrossRef]
25. Kjellberg, M.; Janson, C.E.; Contento, G. Fully Nonlinear Potential Flow Method for Three-Dimensional Body Motion. In Proceedings of the NAV 2012, 17th International Conference on Ships and Shipping Research, Naples, Italy, 17–19 October 2012; p. 117.
26. Zhang, B.J.; Ning, X. The research of added resistance in waves based on nonlinear time-domain potential flow theory. *J. Mar. Sci. Technol.* **2018**, *26*, 343–351.
27. Crepier, P.; Rapuc, S.; Dallinga, R.P. CFD Investigation into the Wave Added Resistance of Two Ships. In Proceedings of the 14th International Symposium on Practical Design of Ships and Other Floating Structures (PRADS 2019), Yokohama, Japan, 22–26 September 2019; Springer: Singapore, 2019; p. 63. [CrossRef]
28. Dai, Y.Z.; Wu, G.X. Time Domain Computation of Large Amplitude Body Motion with the Mixed Source Formulation. In Proceedings of the 8th ICHD, Nantes, France, 30 September–3 October 2008; pp. 441–452.
29. Liu, S.; Papanikolaou, A.; Zaraphonites, G. Prediction of Added Resistance of Ships in Waves. *J. Ocean Eng.* **2011**, *38*, 641–650. [CrossRef]
30. Yang, Y.; Zhu, R.; Hong, L. A frequency-domain hybrid HOBEM for motion responses and added resistance of ships sailing in head and oblique waves. *Ocean Eng.* **2019**, *194*, 106637. [CrossRef]
31. Chen, S.; Hino, T.; Ma, N.; Gu, X. RANS investigation of influence of wave steepness on ship motions and added resistance in regular waves. *J. Mar. Sci. Technol.* **2018**, *23*, 991–1003. [CrossRef]
32. Hirt, C.W.; Nichols, B.D. Volume of fluid (VOF) method for the dynamics of free boundaries. *J. Comput. Phys.* **1981**, *39*, 201–225. [CrossRef]
33. Sussman, M.; Smereka, P.; Osher, S. A Level Set Approach for Computing Solutions to Incompressible Two-Phase Flow. *J. Comput. Phys.* **1994**, *114*, 146–159. [CrossRef]
34. Deng, G.B.; Leroyer, A.; Guilmineau, E.; Queutey, P.; Visonneau, M.; Wackers, J. Verification, and validation for unsteady computation. In Proceedings of the Gothenburg 2010: A Workshop on CFD in Ship Hydrodynamics, Gothenburg, Sweden, 8–10 December 2010.
35. Sadat-Hosseini, H.; Wu, P.-C.; Carrica, P.M.; Kim, H.; Toda, Y.; Stern, F. CFD verification and validation of added resistance and motions of KVLCC2 with fixed and free surge in short and long head waves. *Ocean Eng.* **2013**, *59*, 240–273. [CrossRef]

36. Sigmund, S.; el Moctar, O. Numerical and experimental investigation of added resistance of different ship types in short and long waves. *Ocean Eng.* **2018**, *147*, 51–67. [CrossRef]
37. Bekhit Bekhit, A.; Lungu, A. Numerical Simulation for Predicting Ship Resistance and Vertical Motions in Regular Head Waves. ASME 2019. In Proceedings of the 38th International Conference on Ocean, Offshore and Arctic Engineering, OMAE 2019, Glasgow, Scotland, 9–14 June 2019.
38. Mikkelsen, H.; Shao, Y.; Walther, J.H.H. CFD verification and validation of added resistance and seakeeping response in regular oblique waves with varying wave length. In Proceedings of the 9th Conference on Computational Methods in Marine Engineering, Virtual, 2–4 June 2021. Paper 176. [CrossRef]
39. Kobayashi, H.; Kume, K.; Orihara, H.; Ikebuchi, T.; Aoki, I.; Yoshida, R.; Yoshida, H.; Ryu, T.; Arai, Y.; Katagiri, K.; et al. Parametric study of added resistance and ship motion in head waves through RANS: Calculation guideline. *Appl. Ocean Res.* **2021**, *110*, 102573. [CrossRef]
40. Vossers, G.; Swaan, W.A.; Rijken, H. Experiments with Series 60 Models in Waves. *Int. Shipbuild. Prog.* **1961**, *8*, 201–232. [CrossRef]
41. Vossers, G.; Swaan, W.A.; Rijken, H. Vertical and Lateral Bending Moment Measurements on Series 60 Models. *Int. Shipbuild. Prog.* **1961**, *8*, 302–320. [CrossRef]
42. Sibul, O.J. *Ship Resistance in Uniform Waves*; Institute of Engineering Research Report No. NA-64-1; University of California: Berkeley, CA, USA, 1964.
43. Sibul, O.J. *Measurements and Calculations of Ship Resistance in Waves*; University of California, College of Engineering, Report No. NA-71-2; University of California: Berkeley, CA, USA, 1971.
44. Longo, J.; Stern, F. Uncertainty assessment for towing tank tests with example for surface combatant DTMB Model 5415. *J. Ship Res.* **2005**, *49*, 55–68. [CrossRef]
45. Irvine, M.; Longo, J.; Stern, F. Pitch and heave tests and uncertainty assessment for a surface combatant in regular head waves. *J. Ship Res.* **2008**, *52*, 146–163. [CrossRef]
46. Park, D.-M.; Lee, J.; Kim, Y. Uncertainty analysis for added resistance experiment of KVLCC2 ship. *Ocean Eng.* **2015**, *95*, 143–156. [CrossRef]
47. Sogihara, N.; Tsujimoto, M.; Fukasawa, R.; Hamada, T. Uncertainty analysis for measurement of added resistance in short regular waves: Its application and evaluation. *Ocean Eng.* **2020**, *216*, 107823. [CrossRef]
48. Saettone, S.; Taskar, B.; Steen, S.; Andersen, P. Experimental measurements of propulsive factors in following and head waves. *Appl. Ocean Res.* **2021**, *111*, 102639. [CrossRef]
49. Hirota, K.; Matsumoto, K.; Takagishi, K.; Orihara, H.; Yoshida, H. Verification of Ax-Bow Effect based on Full Scale Measurement. *J. Kansai Soc. Nav. Archit. Jpn.* **2004**, *241*, 33–40.
50. Kuroda, M.; Tsujimoto, M.; Sasaki, N.; Ohmatsu, S.; Takagi, K. Study on the bow shapes above the waterline in view of the powering and green-house gas emissions in actual seas. *J. Eng. Marit. Environ.* **2011**, *226*, 23–35.
51. Lee, J.; Park, D.M.; Kim, Y. Experimental investigation on the added resistance of modified KVLCC2 hull forms with different bow shapes. *Proc. Inst. Mech. Eng. Part M J. Eng. Marit. Environ.* **2017**, *231*, 395–410. [CrossRef]
52. Yasukawa, H.; Masaru, T. Impact of bow shape on added resistance of a full hull ship in head waves. *Ship Technol. Res.* **2020**, *67*, 136–147. [CrossRef]
53. Hengelmolen, V.; Wellens, P.R. An Experimental Study on Added Resistance Focused on the Effects of Bow Wave Breaking and Relative Wave Measurements. *Int. Shipbuild. Prog.* **2022**, *69*, 61–89. [CrossRef]
54. Martić, I.; Degiuli, N.; Farkas, A.; Gospić, I. Evaluation of the effect of container ship characteristics on added resistance in waves. *J. Mar. Sci. Eng.* **2020**, *8*, 696. [CrossRef]
55. Shigunov, V.; el Moctar, O.; Papanikolaou, A.; Potthoff, R.; Liu, S. International benchmark study on numerical simulation methods for predictions of manoeuvrability of ships in waves. *Ocean Eng.* **2018**, *165*, 365–385. [CrossRef]
56. Seo, M.G.; Park, D.M.; Yang, K.K.; Kim, Y. Comparative study on computation of ship added resistance in waves. *Ocean Eng.* **2013**, *73*, 1–15. [CrossRef]
57. Seo, M.G.; Ha, Y.J.; Nam, B.W.; Kim, Y. Experimental and Numerical Analysis of Wave Drift Force on KVLCC2 Moving in Oblique Waves. *J. Mar. Sci. Eng.* **2021**, *9*, 136. [CrossRef]
58. Lee, J.-H.; Kim, Y.; Kim, B.-S.; Gerhardt, F. Comparative study on analysis methods for added resistance of four ships in head and oblique waves. *Ocean Eng.* **2021**, *236*, 109552. [CrossRef]
59. Yasukawa, H.; Matsumoto, A.; Ikezoe, S. Wave height effect on added resistance of full hull ships in waves. *J. Jpn. Soc. Nav. Archit. Ocean Eng.* **2016**, *23*, 45–54.
60. Dallinga, R. *Ability to Predict the Added Resistance of Ships in Waves Has Matured*; MARIN Report 126; Maritime Research Institute Netherlands: Wageningen, The Netherlands, 2019.
61. Martić, I.; Chillcce, G.; Tello Ruiz, M.; Ramirez, J.; Degiuli, N.; Ould el Moctar, B. Numerical assessment of added resistance in waves of the DTC container ship in finite water depths. In Proceedings of the 5th Mashcon. Knowledge Centre for Manoeuvring in Shallow and Confined Water, Ostend, Belgium, 19–23 May 2019; pp. 273–283.
62. Martić, I.; Degiuli, N.; Majetić, D.; Farkas, A. Artificial neural network model for the evaluation of added resistance of container ships in head waves. *J. Mar. Sci. Eng.* **2022**, *9*, 826. [CrossRef]
63. Martić, I.; Degiuli, N.; Farkas, A.; Grlj, C.G. The application of ANN in estimating added resistance of container ships in regular head waves. In *Sustainable Development and Innovations in Marine Technologies*; CRC Press: Boca Raton, FL, USA, 2022; pp. 175–182.

64. Moctar, E.; Shigunov, O. Zorn Duisburg Test Case: Post-panamax container ship for benchmarking. *Ship Technol. Res. Schiffstechnik* **2012**, *59*, 50–64. [CrossRef]
65. International Towing Tank Conference. *Uncertainty Analysis, Example for Propulsion Test. ITTC—R. P. & G. 7.5-02-03-01.2*; International Towing Tank Conference: Zürich, Switzerland, 2017.
66. International Towing Tank Conference. Propeller model accuracy. In *ITTC Recommended Procedures and Guidelines 7.5-01-02-02*; International Towing Tank Conference: Zürich, Switzerland, 2017.
67. Saettone, S.; Lopez-Olocco, T.; Medina-Manuel, A.; Taskar, B.; Steen, S.; Andersen, P. Experimental measurements of propulsive factors in regular deep-water following waves for a fishing trawler. *Ocean Eng.* **2022**, *263*, 112167. [CrossRef]
68. Shipflow 7. Available online: www.flowtech.se/company/news/194-shipflow-7-0-release (accessed on 5 September 2022).
69. Irannezhad, M.; Eslamdoost, A.; Kjellberg, M.; Bensow, R.E. Investigation of ship responses in regular head waves through a Fully Nonlinear Potential Flow approach. *Ocean Eng.* **2022**, *246*, 110410. [CrossRef]
70. Coslovich, F.; Janson, C.-E.; Kjellberg, M. Prediction of Parametric Rolling for a Container Ship in Regular and Irregular Waves Using a Fully Nonlinear Time Domain Potential Flow Method. In Proceedings of the 8th International Conference on Computational Methods in Marine Engineering, Gothenburg, Sweden, 13–15 May 2019; pp. 646–657.
71. International Towing Tank Conference (ITTC). *Uncertainty Analysis in CFD Verification and Validation Methodology and Procedures 7.5-03-01-01*; International Towing Tank Conference (ITTC): Zürich, Switzerland, 2017; pp. 1–13. Available online: https://www.ittc.info/media/8153/75-03-01-01.pdf (accessed on 10 November 2022).
72. Liu, S.; Papanikolaou, A. Regression analysis of experimental data for added resistance in waves of arbitrary heading and development of a semi-empirical formula. *Ocean Eng.* **2020**, *206*, 107357. [CrossRef]
73. Choi, B.; Wellens, P.R.; Huijsmans, R.H.M. Experimental assessment of effects of bow-wave breaking on added resistance for the fast ship. *Int. Shipbuild. Prog.* **2019**, *66*, 111–143. [CrossRef]
74. Choi, B.; Huijsmans, R.H.M. An analysis method to evaluate the added resistance in short waves considering bow wave breaking. In Proceedings of the 12th International Conference on Hydrodynamics, Egmond aan Zee, The Netherlands, 18–23 September 2016.
75. Journee, J.M.J. *Motions and Resistance of a Ship in Regular Head Waves*; Ship Hydromechanics Laboratory, Delft University of Technology: Delft, The Netherlands, 1976; Report; Volume 428.
76. Chen, C.; Liu, Y.-D.; He, Y.-P.; Chen, Z.; Zheng, G.-Y. Numerical analysis of added resistance in head waves on a Polar Research Vessel and conventional ships. *Ocean Eng.* **2021**, *233*, 108888. [CrossRef]
77. Liu, S.; Sprenger, F.; Papanikolaou, A.; Dafermos, G.; Zaraphonitis, G. Experimental and numerical studies on linear and nonlinear seakeeping phenomena of the DTC ship in regular waves. *Ship Technol. Res. (Schiffstechnik)* **2021**, *68*, 41–61. [CrossRef]